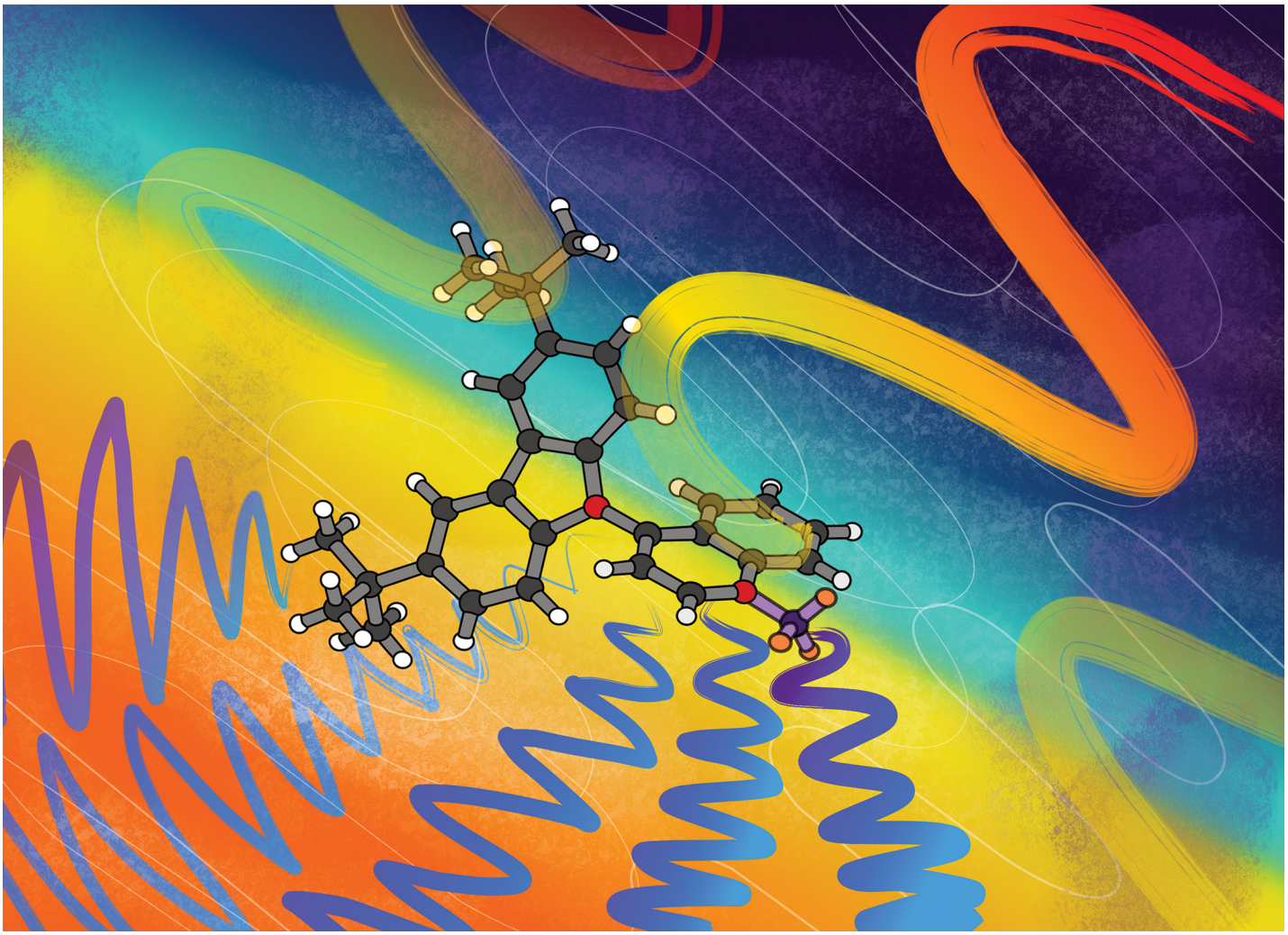

This work is collaborative research between the University of Glasgow, Northumbria University and Durham University.

From phosphorescence to delayed fluorescence in one step: tuning photophysical properties by quaternisation of an sp^2-hybridised nitrogen atom

Introducing a methyl group on the sp^2 nitrogen atom of the aromatic heterocyclic moiety is an easy way to tune the photophysical properties of a material.

As featured in:

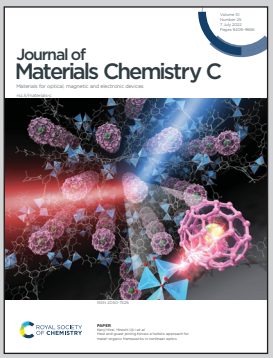

See Peter J. Skabara, Marc K. Etherington *et al.*, *J. Mater. Chem. C*, 2022, **10**, 9484.

ROYAL SOCIETY OF CHEMISTRY

rsc.li/materials-c

Registered charity number: 207890

Journal of Materials Chemistry C

ROYAL SOCIETY OF CHEMISTRY

PAPER

View Article Online
View Journal | View Issue

Cite this: J. Mater. Chem. C, 2022, 10, 9484

From phosphorescence to delayed fluorescence in one step: tuning photophysical properties by quaternisation of an sp^2-hybridised nitrogen atom†

Anastasia Klimash, [a] Antonio Prlj, [bc] Dmitry S. Yufit, [b] Abhijit Mallick, [b] Basile F. E. Curchod, [bc] Paul R. McGonigal, [b] Peter J. Skabara *[a] and Marc K. Etherington *[de]

Received 27th April 2022,
Accepted 23rd May 2022

DOI: 10.1039/d2tc01737g

rsc.li/materials-c

Control of the delayed emission of organic compounds is an important factor in the development of new display technology and for the emerging use of organic emitters in sensing and fluorescence microscopy. In particular, there is a need to understand how the phenomena of room-temperature phosphorescence and thermally activated delayed fluorescence intersect. Here, we show that delayed fluorescence can be activated in room temperature phosphorescence emitters by quaternising the sp^2-hybridised heterocyclic nitrogens. Furthermore by judicious positioning of a carbazole donor in the *meta*- or *para*-position with respect to the ring nitrogen atom, structural and sterical influences combine to tune the origins of the delayed fluorescence from triplet–triplet annihilation to thermally activated delayed fluorescence. Crucially, the quaternisation of nitrogen provides us with the means to fine-tune singlet and triplet states in a predictable manner, uncover the intersection between phosphorescence and delayed fluorescence and tip the balance in favour of delayed fluorescence.

Introduction

For a relatively young field of materials science, organic electronics has attracted significant interest from researchers across the globe and thousands of novel semiconducting organic materials have already been reported.[1–3] For many of these compounds the preparation involves complex multi-step syntheses that are time-consuming and require tedious purification methods. These issues provide limitations to the scale-up of the materials and their use in commercial products. Finding pathways for the preparation of highly efficient compounds that use readily available starting materials and simple synthetic routes would avoid these issues and be beneficial for the field.

It is particularly tempting to discover candidates for use in organic light-emitting diodes (OLEDs) and other optoelectronic and photonic applications among already existing fluorescent materials and then control their properties by simple chemical modifications. Recently it was shown that the quaternisation of one or both nitrogen atoms of quinine, a well-known alkaloid naturally occurring in cinchona trees, leads to significant changes in its emission profile.[4]

This initial work provides a platform to explore the quaternisation of a range of amines with tertiary nitrogen atoms in their aromatic units and highlights a stepwise method with which to alter the photophysical properties of a compound. As a result, numerous readily available natural compounds containing heteroaromatic rings could be modified by this simple procedure and can potentially demonstrate a drastic change in their photophysical properties. Moreover, it might be a promising strategy for inducing phenomena such as thermally activated delayed fluorescence (TADF).[5–8] Initially TADF was observed in Eosin-Y (hence also being known as E-type delayed fluorescence),[9] a material that, similar to quinine, has a protonation site. Protonation and quaternisation have been shown[4,10] to have a significant impact on the behaviour of the charge-transfer (CT) states—states that are crucial to TADF. Quaternisation, therefore, provides an attractive means to explore the control and modification of delayed fluorescence in quinine and similar compounds such as quinoline.

[a] WestCHEM, School of Chemistry, University of Glasgow, University Ave, Glasgow, G12 8QQ, UK. E-mail: Peter.Skabara@glasgow.ac.uk
[b] Department of Chemistry, Durham University, South Road, DH1 3LE, UK
[c] School of Chemistry, University of Bristol, Cantock's Close, Bristol, BS8 1TS, UK
[d] Department of Physics, Durham University, South Road, DH1 3LE, UK
[e] Department of Mathematics, Physics and Electrical Engineering, Northumbria University, Ellison Place, Newcastle upon Tyne, NE1 8ST, UK. E-mail: marc.k.etherington@northumbria.ac.uk

† Electronic supplementary information (ESI) available. CCDC 2149620–2149624. For ESI and crystallographic data in CIF or other electronic format see DOI: https://doi.org/10.1039/d2tc01737g

Compounds containing heterocyclic aromatic moieties with a sp^2-hybridised ring nitrogen are commonplace and include molecules such as quinoline, pyridine and their derivatives. Quinoline has already been exploited as an acceptor motif in a TADF emitter. A carbazole group was introduced at the 8-position of the quinoline, and naphthyl moieties are situated in 2- and 4-positions.[11] Pyridine, in its turn, was only used in TADF materials as a fragment of a larger electron-accepting moiety combined with either benzoyl linkers or triazine.[12,13] There is a significant wealth of literature on the photophysical behaviour of quaternised pyridine derivatives. For instance, 4,4′-bipyridinium salts, also called viologens, exhibit electrochromism.[14,15] The properties of these materials can be easily tuned chemically and electrochemically, which makes them good candidates to use in organic field-effect transistors and for energy storage.[16–18] Similarly, quinolines change their properties significantly when quaternised. For example, Hancock *et al.* reported a quinoline-based fluorescent emitter where the luminescence was modulated by protonation of its nitrogen atoms by camphorsulfonic acid.[19] Work on materials containing *N*-alkylated quinoline has demonstrated that such compounds also show second-order nonlinear optical responses with good characteristics for terahertz wave generation.[20] Quinolinium salts, therefore, provide an easily accessible starting point to uncover new optical properties and have even been shown to exhibit aggregation-induced emission (AIE) behaviour,[21–23] opening a pathway to non-doped OLED architectures.[24]

Here we present a series of quaternised quinoline-based donor–acceptor compounds and reveal that such compounds provide access to delayed fluorescence. There has been recent interest in the switching between room temperature phosphorescence (RTP) and TADF and the interplay between these phenomena.[25–28] The alkylation step tunes the energy levels in such a fashion to induce either TADF or triplet–triplet annihilation (TTA) from two room temperature phosphorescence (RTP) materials. Additionally, the quinolinium-based materials presented in this work demonstrate AIE and mechanochromism (MC) meaning they have potential for both functional and photonic applications. There has been significant recent interest in the study of materials that simultaneously exhibit TADF, AIE and MC[29–31] and while not the only TADF-active salts,[32–34] to our knowledge, these compounds are the first organic salts that are prepared from non-TADF materials to show all three. To summarise, the modification of known N-heterocyclic chromophores by quaternisation provides rapid access to new materials with altered charge transfer and emission properties.

Results and discussion

Synthesis

To investigate the influence of quaternisation on the photophysical properties of quinoline-based donor–acceptor materials, we synthesised two new compounds, **Q1** and **Q2** (Scheme 1). Here, 3,6-di-*tert*-butylcarbazole (^{t}Bu-CBZ) was introduced as a donor in the 3- or 4-position of quinoline. The compounds were then methylated to prepare (Scheme 1) a series of quinoline salts **MeQ1**·X and **MeQ2**·X with triflate, iodide or tetrafluoroborate as the anion, X.

Both **Q1** and **Q2** were prepared *via* Buchwald–Hartwig coupling between 3,6-di-*tert*-butylcarbazole and 3-bromoquinoline (**1**) or 4-bromoquinoline (**2**), respectively. Compounds **MeQ1**·X and **MeQ2**·X were prepared by the methylation of **Q1** and **Q2**, respectively, with corresponding methylating agents (Scheme 1). For the preparation of tetrafluoroborate salts **MeQ1**·BF_4 and **MeQ2**·BF_4, we followed the synthetic procedure previously reported by Kim *et al.*[35] for the synthesis of imidazolium ionic liquids. We modified the procedure for use in a microwave to reduce reaction times. This method allows for direct alkylation of **Q1** and **Q2**, without the need of an anion exchange step, and uses trimethyl orthoformate as a more environmentally friendly alternative to the standard *N*-methylating agents. This procedure will be further explored in our future work. General synthetic characterisation such as electrochemistry and thermal analysis can be found in the ESI† (Fig. S1–S20 and Tables S1, S2).

Photophysical characterisation

Steady-state photoluminescence and absorption in solution. The steady-state photoluminescence and absorption spectra were measured for **Q1**, **Q2**, **MeQ1**·OTf and **MeQ2**·OTf across a series of solvents with different polarities. The triflate salt was the main focus of our investigation as the absorption and photoluminescence profiles for the salts with different counter-ions were very similar. As expected from our previous work[4] there was a significant red shift in the absorption spectra in going from the **Q1** and **Q2** compounds to their respective

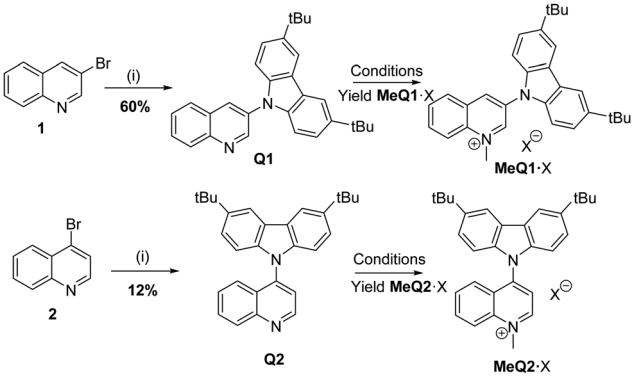

X	OTf	I	BF_4
Conditions	(ii)	(iii)	(iv)
Yield MeQ1·X, %	82	60	54
Yield MeQ2·X, %	72	52	48

Scheme 1 General strategy for the preparation of the series of *N*-alkylated quinoline-based compounds **MeQ1**·X and **MeQ2**·X. (i) 3,6-Di-*tert*-butylcarbazole, XPhos, $Pd_2(dba)_3$, NaO^tBu, PhMe, 110 °C, 18 h; (ii) MeOTf, CH_2Cl_2, 0 °C to rt, 10 h; (iii) MeI, PhMe, 100 °C, microwave, 3 h; (iv) NH_4BF_4, $(MeO)_3CH$, 110 °C, microwave, 1 h. dba = dibenzylideneacetone; OTf = triflate.

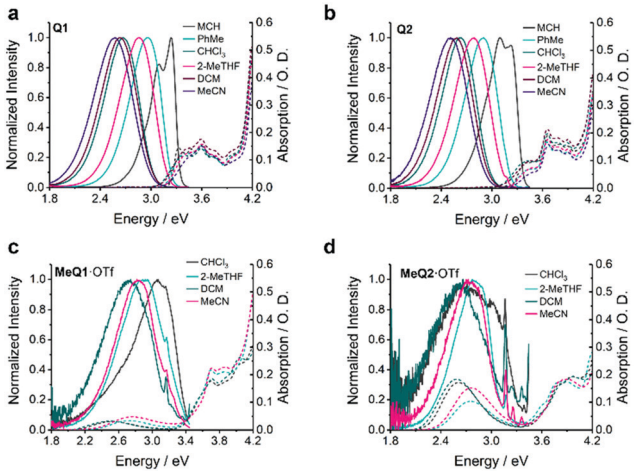

Fig. 1 Steady-state photoluminescence (solid) and absorption (dash) spectra of (a) **Q1**, (b) **Q2**, (c) **MeQ1**·OTf and (d) **MeQ2**·OTf in a series of solvents.

salts. A large red shift in absorption of the methylated species (**MeQ1**$^+$ and **MeQ2**$^+$) is also predicted by theoretical calculations employing SCS-ADC(2)/def2-SVP method (see ESI† for details) which are performed in vacuum (Table S8, ESI†).

The emission and absorption for **Q1** and **Q2** were investigated in solutions of methylcyclohexane (MCH), toluene (PhMe) chloroform ($CHCl_3$), 2-methyltetrahydrofuran (2-MeTHF), dichloromethane (DCM) and acetonitrile (MeCN) at 20 μM concentrations (see Fig. 1 and Fig. S21, ESI†).

The absorption spectra for **Q1** and **Q2** in most solvents demonstrate two strong bands corresponding to π–π* transitions with several additional smaller peaks (Fig. 1 and Fig. S21, Table S3, ESI†). The two main bands are consistent with calculations, which indicate that the lower intense band of both compounds mainly correspond to a moderate CT transition, while the higher energy intense band comes from a LE state localised on carbazole (Table S8, ESI†).

Q1 is a blue emitter and, as expected for donor–acceptor compounds, it undergoes a bathochromic shift of up to 0.35 eV (from MCH to MeCN) in its photoluminescence onset with increasing solvent polarity. This is indicative of the CT character of the emission (Fig. 1 and Fig. S21, Table S4, ESI†). The emission peak of **Q2** in MCH is slightly red-shifted compared to **Q1** but the onsets are similar. **Q2** also exhibits similar bathochromic shifts in its photoluminescence onset (0.45 eV from MCH to MeCN) with increasing solvent polarity (Table S4, ESI†).

Interestingly, upon methylation the compounds become almost non-emissive in solution and, therefore, only weak emission spectra could be recorded in solution for **MeQ1**·OTf and **MeQ2**·OTf (see Fig. 1 and Fig. S22, ESI†). This indicates the presence of nonradiative decay channels quenching the emission in solution.

The methylated compounds are insoluble in MCH, so the spectra were recorded in 2-MeTHF, DCM, $CHCl_3$ and MeCN. Similar to **Q1**, the absorption spectra of **MeQ1**·OTf exhibits several absorption peaks between 4.28 eV (290 nm) and 3.71 eV (334 nm). A new CT band emerges at a longer wavelength (around 2.76 eV (450 nm) in 2-MeTHF and MeCN, Fig. 1 and Fig. S22, Table S3, ESI†). The last band demonstrates a red shift of almost 0.29 eV in DCM and $CHCl_3$ (peak at 2.47 eV (502 nm)) compared to the 2-MeTHF and MeCN solutions. **MeQ2**·OTf demonstrates very similar behaviour. It exhibits a new CT band around 2.76 eV (450 nm) in 2-MeTHF and MeCN that is similarly red-shifted in DCM (0.16 eV to 2.60 eV (477 nm)) and $CHCl_3$ (0.18 eV to 2.58 eV (480 nm)) (Fig. 1 and Fig. S22, Table S3, ESI†). Strong CT character of the lowest excited singlet state is also predicted by calculations for both compounds (*i.e.* cations in vacuum, see Table S8, ESI†).

All **MeQ1**$^+$ and **MeQ2**$^+$-based salts demonstrate very similar absorption and emission profiles, so most of the measurements were performed only for **MeQ1**·OTf and **MeQ2**·OTf compounds. The salts only become emissive in an aggregated state, indicative of their AIE character (see Fig. 2). Aggregation is known to restrict and inhibit deleterious nonradiative decay channels, simply by limiting molecular motions which lead to such deactivation processes.[36,37] It is also possible that in solid state the molecules are predominantly adopting a more emissive conformation.

Due to the non-emissive nature of the salts in well-dissolved solutions, we confirmed their AIE behaviour using solvent mixtures of tetrahydrofuran (THF) and hexane (see Fig. 2). As the compounds are insoluble in hexane, the addition of hexane to the THF solutions causes the compounds to form aggregates and activate their AIE. The intensity of the emission increases for both **MeQ1**·OTf and **MeQ2**·OTf with the increase in volume fraction of hexane (f_{hex}).

Steady-state photoluminescence and absorption in the solid state. Having established the AIE characteristics of the salts, all subsequent photophysical characterisation was performed on thin films in the solid state to capture the differences between the original compounds and the salts (see Table 1 for a key summary of photophysical results). The steady-state photoluminescence and absorption spectra were recorded for all eight materials as films in which 1 wt% of the compound is dispersed in the poly(methyl methacrylate) (PMMA) matrix (see Fig. S23 and S24, ESI†).

Absorption spectra of materials **Q1** and **Q2** in PMMA films (Fig. S23 and Table S5, ESI†) are very similar to those recorded

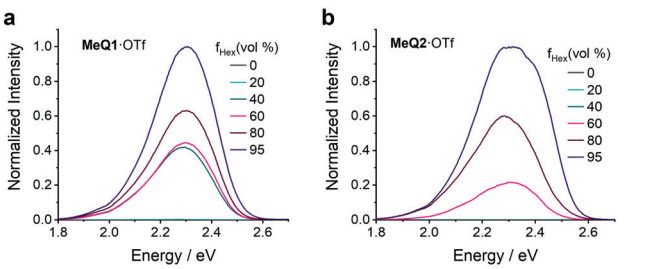

Fig. 2 Photoluminescence spectra of (a) **MeQ1**·OTf and (b) **MeQ2**·OTf in THF/hexane mixtures with different hexane fractions (f_{Hex}). The excitation wavelength is 450 nm.

Table 1 Key photophysical parameters of the **Q1**, **Q2**, **MeQ1**·OTf and **MeQ2**·OTf compounds

Compound	Emission peak[a]/eV	PLQY[ab]/%	ΔE_{S-T}[ac]/eV
Q1	3.03	20	0.57
Q2	2.99	19	0.57
MeQ1·OTf	2.12 (2.16)	4 (13)	0.14 (0.28)
MeQ2·OTf	2.10 (2.13)	13 (34)	0.06 (0.11)

[a] In 1 wt% PMMA with neat film values in brackets. [b] Measured in air. [c] Experimentally obtained from the onsets of the prompt fluorescence and phosphorescence spectra.

in solution (Fig. S21 and Table S3, ESI†) and both feature the two main bands consistent with the calculations (Table S8, ESI†). As with the solution measurements, several smaller peaks are also observed and are detailed in Table S5 (ESI†). Both **Q1** and **Q2** emit light in the blue region of the spectrum with peaks at 3.05 eV (407 nm) and 3.01 eV (412 nm), respectively (Fig. S23 and Table S5, ESI†). The photoluminescence quantum yields (PLQYs) of the two materials in PMMA are approximately 20% (Table 1).

The absorption spectra for the **MeQ1** salts are nearly identical, independent of the nature of the counter-ion (Fig. S24 and Table S5, ESI†). **MeQ2** derivatives demonstrate similar behaviour (Fig. S24 and Table S5, ESI†). All six salts are yellow emitters with photoluminescence peaks between 2.15 eV (578 nm) and 2.10 eV (590 nm) (Fig. S24 and Table S5, ESI†). The methylation of the aromatic quinoline unit has therefore had a significant effect on the colour of the photoluminescence. This observation is consistent with the behaviour observed upon methylating quinine,[4] although with a more drastic energy shift.

For compounds **MeQ1**·OTf and **MeQ2**·OTf, PLQYs were recorded as both 1 wt% PMMA dispersions and as neat films. The emission is largely quenched in the PMMA matrix for both **MeQ1**·OTf (13% in neat film and 4% in PMMA) and **MeQ2**·OTf (34% in neat film and 13% in PMMA) (see Table 1). This is due to the aggregation-induced nature of the emission of the materials. The restriction of molecular motion increases from solution to PMMA matrix to neat film. This inhibits the non-radiative decay, hence the increase of PLQY. The more than twofold increase of PLQY for **MeQ2**·OTf compared to **MeQ1**·OTf is in correlation with the theoretical findings indicating a higher oscillator strength for the S_1 of $\mathbf{MeQ2}^+$ (0.263) compared to $\mathbf{MeQ1}^+$ (0.051, Table S8, ESI†), which is also apparent from the relative intensity of the CT band in the absorption spectra (Fig. 1 and Fig. S24, ESI†).

All salts exhibit mechanochromism, *i.e.* their colours change after mechanical force is applied. Due to the quenching of luminescence in **MeQ1**·I and **MeQ2**·I in the solid-state, mechanochromism was only investigated for the OTf and BF_4 salts. Initially all four materials are yellow emitters that, after grinding, exhibit shifts in their photoluminescence to the red region (Fig. S25, S26 and Table S6, ESI†). The $\mathbf{MeQ1}^+$ salts, **MeQ1**·OTf and **MeQ1**·BF_4, demonstrate much smaller PL peak shifts of 0.11 eV and 0.08 eV, compared to **MeQ2**·OTf (0.19 eV) and **MeQ2**·BF_4 (0.24 eV). This suggests that when ^{t}Bu-CBZ is in the 4-position of the quinoline ring, the material exhibits more significant changes in the packing after grinding than when ^{t}Bu-CBZ is in the 3-position.

Time-resolved photoluminescence in the solid state. Due to the oxygen dependent nature of RTP and TADF all of the time-resolved photoluminescence measurements were performed in an oxygen-free environment. Time-resolved measurements were first performed in neat films of **MeQ1**·OTf and **MeQ2**·OTf. Both compounds show delayed emission at room temperature (RT) (Fig. 3 and Fig. S27, S28, ESI†). For **MeQ1**·OTf the lifetime of prompt fluorescence (~28 ns) and delayed fluorescence (~9 μs) are longer than those for **MeQ2**·OTf (around 15 ns and 7 μs, respectively).

To give further comparison between the starting materials **Q1** and **Q2** and the salts, time-resolved photoluminescence measurements were also performed on 1 wt% PMMA films (see Fig. 4 and Fig. S29–S32, ESI†). These measurements confirm the room temperature phosphorescence (RTP) nature of **Q1** and **Q2** and demonstrate that upon alkylation, the RTP is tuned to delayed fluorescence. In a simple, single synthetic step, we have converted RTP materials into delayed fluorescence emitters with AIE behaviour.

Q1 and **Q2** show clear room temperature phosphorescence in 1 wt% PMMA film. Radiative decay from triplet states of **Q1** and **Q2** is favoured due to the large energy gap between the lowest triplet and the lowest singlet states (Table S8, ESI†). Calculations also predict sufficiently short phosphorescence lifetimes of 0.86 s and 1.35 s, respectively, for **Q1** and **Q2** giving additional confirmation that RTP is taking place in these compounds. Quaternisation significantly tunes the singlet and triplet levels – in methylated compounds the singlet–triplet energy gap (ΔE_{S-T}) is reduced, opening up the possibility for delayed fluorescence due to reverse intersystem crossing from a triplet to singlet state. This change from RTP to delayed

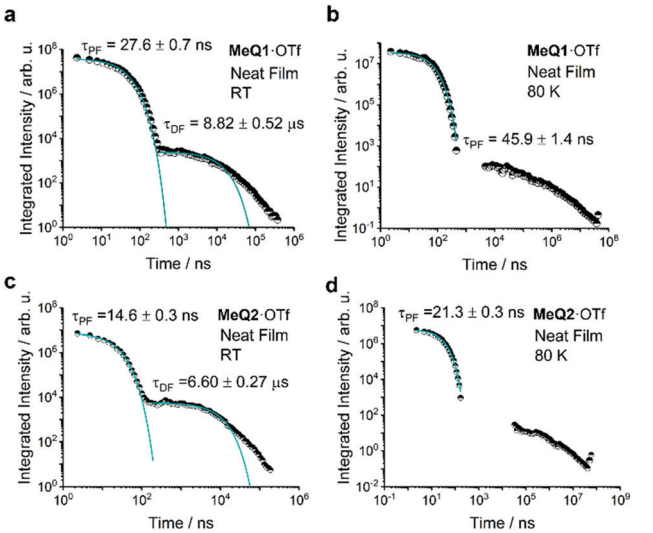

Fig. 3 Time-resolved photoluminescence decays for (a and b) **MeQ1**·OTf and (c and d) **MeQ2**·OTf in neat film at RT and 80 K.

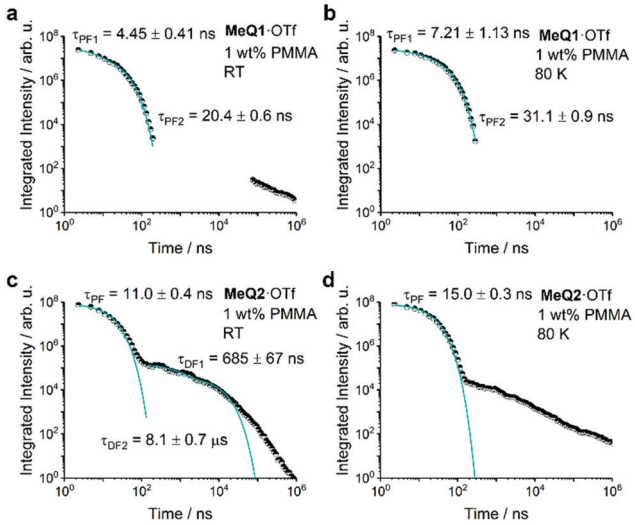

Fig. 4 Photoluminescence decay for (a and b) **MeQ1**·OTf and (c and d) **MeQ2**·Otf in 1 wt% PMMA films at RT and 80 K.

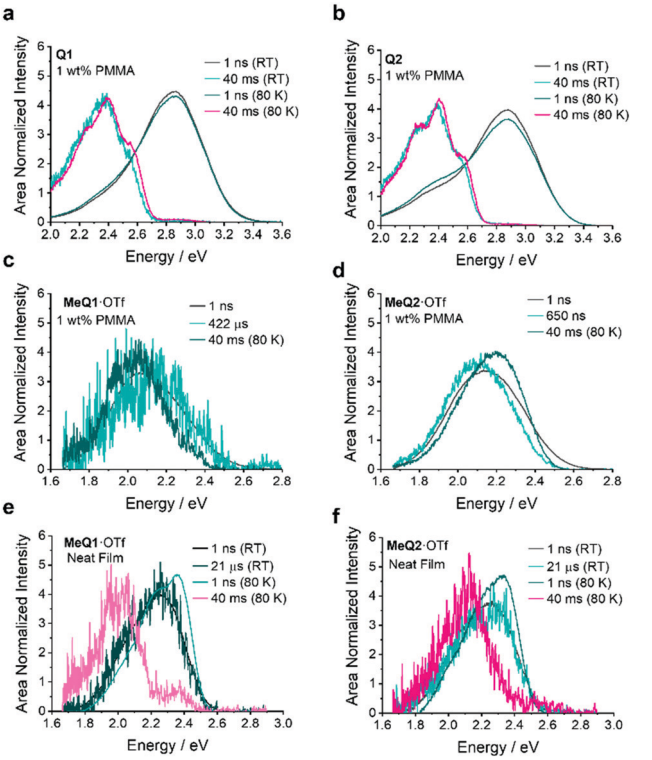

Fig. 5 Time resolved spectra at RT and 80 K for demonstrating the RTP, TADF and TTA characters of (a) **Q1**, (b) **Q2**, (c and e) **MeQ1**·OTf and (d and f) **MeQ2**·OTf.

fluorescence can be quantitatively explained by considering the energetics of the two compounds. The ΔE_{S-T} gaps for **MeQ1**·OTf and **MeQ2**·OTf in both neat films and 1 wt% PMMA film can be estimated from measuring the S_1 and T_1 energies for both samples from the onset of the high energy-edge of the fluorescence and phosphorescence peaks, respectively (Table S7, ESI† and Fig. 5). For the neat films the first singlet excited states S_1 are nearly isoenergetic for **MeQ1**·OTf and **MeQ2**·OTf (2.51 eV), while the energy of the T_1 triplet state is 0.17 eV lower for the **MeQ1**·OTf (2.23 eV) compared to **MeQ2**·OTf (2.40 eV). The ΔE_{S-T} is consequently much smaller for **MeQ2**·OTf (0.11 eV) compared to **MeQ1**·OTf (0.28 eV). Theoretically, the computed ΔE_{S-T} (based on ground-state minimum energy geometries in vacuum) are 0.25 and 0.17 eV for $\mathbf{MeQ1}^+$ and $\mathbf{MeQ2}^+$, respectively. However, we note that estimates of excitation energies from these experimental fluorescence and phosphorescence onsets, or calculations based on fixed ground state geometries, assume that the ΔE_{S-T} can be obtained as in Scheme 2a. However, if there is a difference in geometry between the S_1 and T_1, then the experimental values from measurement of the onset relate instead to Scheme 2b and thus ΔE_{S-T} cannot be obtained directly unless the energy gap due to the change in geometry is also known $(S_0'-S_0)$. As an alternative, we optimised the S_1 and T_1' states of both compounds theoretically as in Scheme 2b. The downside of this approach is that it still corresponds to the situation in vacuum – the molecules have more flexibility as compared to the solid state. Nevertheless, we found that S_1 and T_1' excited state minima are nearly degenerate for $\mathbf{MeQ2}^+$, while in the case of $\mathbf{MeQ1}^+$ the absolute energy of the S_1 minimum is 0.14 eV above the T_1' minimum (Table S10, ESI†). Once again, our results imply that the intersystem crossing may be more easily achieved in $\mathbf{MeQ2}^+$ than $\mathbf{MeQ1}^+$ compounds.

While we have demonstrated that the singlet and triplet states change energy between the original compounds and the

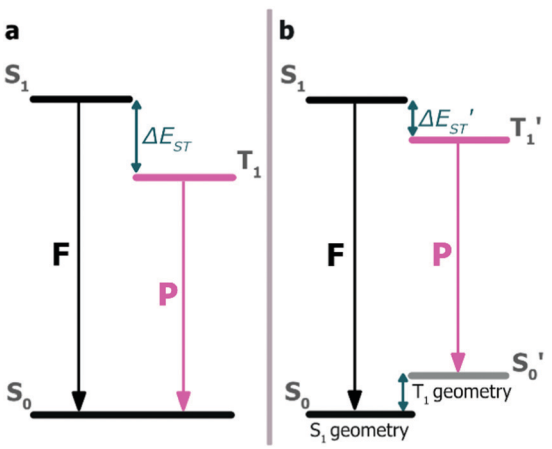

Scheme 2 Relaxation of the lowest singlet and triplet excited states *via* fluorescence (F) and phosphorescence (P), respectively, according to (a) idealised Jablonski scheme where geometry changes are not taken into account and (b) realistic scheme where S_1 and T_1 optimal geometries differ.

salts, explaining why the changes are different between **MeQ1** and **MeQ2** is more complex. The different response to quaternisation for these two compounds is quite a surprising outcome as one would expect **MeQ2**·OTf, with its ^{t}Bu-CBZ group in the *para*-position, to have a better conjugation between the donor and acceptor moieties and thus a larger overlap between

the highest occupied molecular orbital (HOMO) and lowest unoccupied molecular orbital (LUMO) energy levels compared to **MeQ1**·OTf, where the communication between the quinoline nitrogen and the ^{t}Bu-CBZ unit should be partially interrupted by virtue of *meta*-position. The fact that **MeQ2**·OTf is a better TADF emitter, compared to **MeQ1**·OTf, might indicate that other factors can influence the magnitude of the ΔE_{S-T} gap. It is also possible that in the excited state the dihedral angle between the donor and acceptor moieties is larger for **MeQ2**·OTf than it is **MeQ1**·OTf, which leads to a better separation of HOMO and LUMO for the former. Indeed, theoretical excited-state optimisations performed in vacuum predict a significantly larger dihedral angle for the S_1 and T_1' minimum geometries of **MeQ2**$^+$, as compared to the S_1 and T_1' states of **MeQ1**$^+$ (Table S10, ESI†).

As a result of these different changes and, therefore, different energy gaps for **MeQ1**$^+$ and **MeQ2**$^+$, we must consider the origin of the delayed fluorescence. Having imparted the salts with delayed fluorescence it is now possible to determine its origin by measuring the dependence of fluorescence intensity (I_F) on laser fluence (E_{ex}). TTA demonstrates quadratic power dependence at lower excitation dose with the slope n being 2 for $I_F \sim E_{ex}^n$ that turns into 1 at high triplet densities.[38,39] For TADF materials the dependence is always linear, *i.e.*, $n = 1$. To confirm the nature of delayed fluorescence for the quaternised compounds, we performed laser fluence measurements on the neat films of the OTf salts. The estimated slope for the **MeQ1**·OTf salt is 1.29, which indicates that the emission has bimolecular contribution and most likely originates from TTA (Fig. S33, ESI†). For **MeQ2**·OTf, the power dependence is linear, thus the fluorescence originates from TADF (Fig. S33, ESI†). We can also compare the estimated reverse intersystem crossing rates for **MeQ1**·OTf and **MeQ2**·OTf (Table S7, ESI†) showing that **MeQ2**·OTf has an order of magnitude higher rISC rate consistent with its smaller ΔE_{S-T}, larger TADF contribution to the delayed fluorescence and overall better performance as an emitter.

Thus, through a single-step synthesis we have converted one RTP compound into a TADF emitter and a very similar RTP compound into an emitter that exhibits a mixture of TADF and TTA. This demonstrates the level of control that can be exerted over the energetic states of organic chromophores utilising a combination of quaternisation and structural and steric properties (Fig. S40, ESI†).

X-Ray crystallography. Solid-state structures of **MeQ1**·BF_4, **MeQ1**·OTf, **Q2**, **MeQ2**·BF_4 and **MeQ2**·OTf have been determined by single-crystal X-ray crystallography. The unit cells of **MeQ1**·OTf and both **MeQ2**$^+$ salts each contain two crystallographically independent ionic pairs with virtually identical conformations of the organic cations. The BF_4 salts crystallised as solvates containing acetonitrile and disordered water molecules in the cases of **MeQ1**·BF_4 and **MeQ2**·BF_4, respectively (Fig. S34–S36, ESI†). In both the **MeQ1**$^+$ and **MeQ2**$^+$ cations, the two planar donor (^{t}Bu-CBZ) and acceptor (quinoline) polycyclic moieties are significantly twisted relative to each other. The dihedral angle between the mean planes of quinoline and ^{t}Bu-CBZ fragments varies from (50.4(1)° in **MeQ1**·BF_4 to 62.7(1)° (average over two independent cations) in **MeQ1**·OTf. Whereas the dihedral angle observed for **Q2** is 62.38(4)° (Fig. 6 and Table S11, ESI†). These findings are well in line with the theoretically calculated dihedral angles for the ground-state geometries of **Q2**, **MeQ1**$^+$ and **MeQ2**$^+$ (Table S9, ESI†).

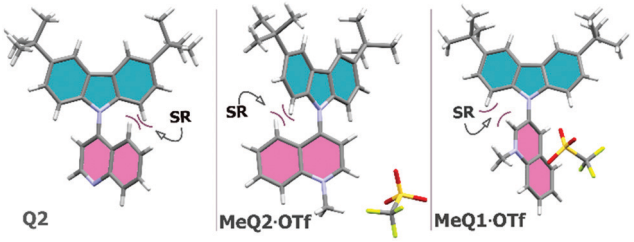

Fig. 6 The X-ray crystal structures of **Q2**, **MeQ2**·OTf and **MeQ1**·OTf. SR = steric repulsion.

In the crystalline state, the minor differences in the conformations of the cations do not affect the lengths of the N–C bonds between the planar donor and acceptor fragments, which is very similar in all studied molecules. The fact that the dihedral angles between the donor and acceptor moieties do not change significantly with the methylation, while the luminescence type changes from phosphorescence to delayed fluorescence, demonstrates that achieving high twist between the donor and acceptor unit is not sufficient for the separation of HOMO and LUMO and consequent reduction of the ΔE_{S-T} gap. Instead, tuning the relative strength of donor and acceptor plays a much more important role. In this case, the methylation of the N-atom on the quinoline unit makes it more electron-deficient, changing the energy gap and inducing delayed fluorescence.

The molecules of **Q2** in the crystalline state are linked by both CH···N and π···π intermolecular interactions (Fig. 7 and Fig. S37, ESI†). On the contrary, π-stacking between the aromatic rings are suppressed in **MeQ2**·OTf and **MeQ1**·OTf on account of the triflate counterion increasing the spacing between each cation (Fig. 7 and Fig. S38, S39, ESI†). This indicates a significant influence of inter-ionic electrostatic

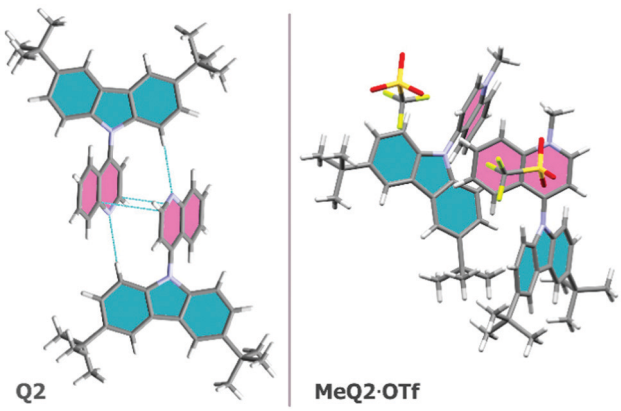

Fig. 7 Face-to-face aromatic intermolecular interactions in **Q2** and their absence in **MeQ2**·OTf from X-ray crystal packing.

interactions on packing motifs in crystal structures of the studied salts. These interactions could also explain why the salts exhibit AIE and mechanochromism. The packing of **MeQ2**·OTf also lacks strong direction-specific interactions between the $\mathbf{MeQ2}^{+}$ units.

Conclusions

To conclude, the materials presented in this work can be prepared *via* a simple two-step synthesis involving a relatively quick purification process to convert RTP emitters into delayed fluorescence, and in particular, TADF emitters. This provides a simple pathway to expand the library of TADF emitters by enhancing already existing molecules without the need to design new molecular motifs from scratch. In total, six new quinoline-based salts were synthesised. Apart from TTA and TADF, the salts demonstrate additional functional behaviour including AIE and mechanochromism.

The tuning of the energy levels by alkylation has been rationalised *via* calculations and experimentally verified through time-resolved photoluminescence measurements. Interestingly while both materials exhibit delayed fluorescence and despite a very similar structure, **MeQ1**·OTf shows a mixture of TADF and TTA while **MeQ2**·OTf is a solely TADF emitter.

Author contributions

A. K.: conceptualisation, formal analysis, investigation, methodology, project administration, resources, visualisation, writing – original draft, writing – review & editing; A. P.: conceptualisation, investigation, formal analysis, software, visualisation, writing – original draft, writing – review & editing; D. S. Y.: investigation, visualisation, writing – original draft, writing – review & editing; A. M.: investigation, writing – review & editing; B. F. E. C.: conceptualisation, formal analysis, software, supervision, writing – review & editing; P. R. M.: conceptualisation, writing – review & editing; P. S.: conceptualisation, supervision, funding acquisition, writing – review & editing; M. K. E.: conceptualisation, formal analysis, investigation, methodology, project administration, resources, supervision, visualisation, writing – original draft, writing – review & editing.

Conflicts of interest

There are no conflicts to declare.

Acknowledgements

This research has received funding from the European Union's Horizon 2020 research and innovation programme under the Marie Skłodowska-Curie grant agreement H2020-MSCA-ITN2015/674990 project ''EXCILIGHT''. A. K. also thanks the EPSRC for funding (EP/T013710/1). M. K. E. thanks the Royal Society of Chemistry (R20-1668) for support. The authors also thank Andrew P. Monkman for use of his facilities for the spectroscopic work.

Notes and references

1 Y. C. Liu, C. S. Li, Z. J. Ren, S. K. Yan and M. R. Bryce, *Nat. Rev. Mater.*, 2018, **3**, 18020.
2 M. Y. Wong and E. Zysman-Colman, *Adv. Mater.*, 2017, 29.
3 H. Nakanotani, Y. Tsuchiya and C. Adachi, *Chem. Lett.*, 2021, **50**, 938–948.
4 A. T. Turley, A. Danos, A. Prlj, A. P. Monkman, B. F. E. Curchod, P. R. McGonigal and M. K. Etherington, *Chem. Sci.*, 2020, **11**, 6990–6995.
5 H. Uoyama, K. Goushi, K. Shizu, H. Nomura and C. Adachi, *Nature*, 2012, **492**, 234–238.
6 M. K. Etherington, J. Gibson, H. F. Higginbotham, T. J. Penfold and A. P. Monkman, *Nat. Commun.*, 2016, **7**, 13680.
7 F. B. Dias, K. N. Bourdakos, V. Jankus, K. C. Moss, K. T. Kamtekar, V. Bhalla, J. Santos, M. R. Bryce and A. P. Monkman, *Adv. Mater.*, 2013, **25**, 3707–3714.
8 J. Gibson, A. P. Monkman and T. J. Penfold, *ChemPhysChem*, 2016, **17**, 2956–2961.
9 C. A. Parker and C. G. Hatchard, *Trans. Faraday Soc.*, 1961, **57**, 1894–1904.
10 J. Qian and A. M. Brouwer, *Phys. Chem. Chem. Phys.*, 2010, **12**, 12562–12569.
11 I. Bhattacharjee, N. Acharya and D. Ray, *Chem. Commun.*, 2019, **55**, 1899–1902.
12 J. Pandidurai, J. Jayakumar, N. Senthilkumar and C. H. Cheng, *J. Mater. Chem. C*, 2019, **7**, 13104–13110.
13 S. J. Yoon, H. J. Lee, K. H. Lee and J. Y. Lee, *J. Mater. Chem. C*, 2020, **8**, 7485–7491.
14 C. J. Schoot, J. J. Ponjee, H. T. van Dam, R. A. van Doorn and P. T. Bolwijn, *Appl. Phys. Lett.*, 1973, **23**, 64–65.
15 P. M. S. Monk, D. R. Rosseinsky and R. J. Mortimer, in *Electrochromic Materials and Devices*, ed. P. M. S. Monk, D. R. Rosseinsky and R. J. Mortimer, 2015, ch, **3**, pp. 57–90.
16 J. C. Barnes, A. C. Fahrenbach, D. Cao, S. M. Dyar, M. Frasconi, M. A. Giesener, D. Benitez, E. Tkatchouk, O. Chernyashevskyy, W. H. Shin, H. Li, S. Sampath, C. L. Stern, A. A. Sarjeant, K. J. Hartlieb, Z. Liu, R. Carmieli, Y. Y. Botros, J. W. Choi, A. M. Slawin, J. B. Ketterson, M. R. Wasielewski, W. A. Goddard, 3rd and J. F. Stoddart, *Science*, 2013, **339**, 429–433.
17 E. M. Kosower and J. L. Cotter, *J. Am. Chem. Soc.*, 2002, **86**, 5524–5527.
18 L. Michaelis, *Chem. Rev.*, 1935, **16**, 243–286.
19 J. M. Hancock and S. A. Jenekhe, *Macromolecules*, 2008, **41**, 6864–6867.
20 S. I. Kim, B. J. Kang, C. U. Jeong, M. H. Shin, W. T. Kim, M. Jazbinsek, W. Yoon, H. Yun, D. Kim, F. Rotermund and O. P. Kwon, *Adv. Opt. Mater.*, 2019, **7**, 1801495.
21 J. Luo, Z. Xie, J. W. Lam, L. Cheng, H. Chen, C. Qiu, H. S. Kwok, X. Zhan, Y. Liu, D. Zhu and B. Z. Tang, *Chem. Commun.*, 2001, 1740–1741.
22 Y. Hong, J. W. Y. Lam and B. Z. Tang, *Chem. Commun.*, 2009, 4332–4353.
23 J. Mei, Y. Hong, J. W. Y. Lam, A. Qin, Y. Tang and B. Z. Tang, *Adv. Mater.*, 2014, **26**, 5429–5479.

24 K. Tanabe, D. Kodama, M. Hasegawa and T. Kato, *Chem. Lett.*, 2014, **43**, 184–186.
25 P. Data, M. Okazaki, S. Minakata and Y. Takeda, *J. Mater. Chem. C*, 2019, **7**, 6616–6621.
26 T. Hosono, N. O. Decarli, P. Z. Crocomo, T. Goya, L. E. de Sousa, N. Tohnai, S. Minakata, P. de Silva, P. Data and Y. Takeda, *J. Mater. Chem. C*, 2022, **10**, 4905–4913.
27 L. Zhan, Z. Chen, S. Gong, Y. Xiang, F. Ni, X. Zeng, G. Xie and C. Yang, *Angew. Chem., Int. Ed.*, 2019, **58**, 17651–17655.
28 N. A. Kukhta, R. Huang, A. S. Batsanov, M. R. Bryce and F. B. Dias, *J. Phys. Chem. C*, 2019, **123**, 26536–26546.
29 M. Okazaki, Y. Takeda, P. Data, P. Pander, H. Higginbotham, A. P. Monkman and S. Minakata, *Chem. Sci.*, 2017, **8**, 2677–2686.
30 S. Xu, T. Liu, Y. Mu, Y. F. Wang, Z. Chi, C. C. Lo, S. Liu, Y. Zhang, A. Lien and J. Xu, *Angew. Chem., Int. Ed.*, 2015, **54**, 874–878.
31 M. K. Etherington, *Front. Chem.*, 2020, **8**, 716.
32 M. Y. Wong, M.-G. La-Placa, A. Pertegas, H. J. Bolink and E. Zysman-Colman, *J. Mater. Chem. C*, 2017, **5**, 1699–1705.
33 M. Y. Wong, G. J. Hedley, G. Xie, L. S. Kölln, I. D. W. Samuel, A. Pertegás, H. J. Bolink and E. Zysman-Colman, *Chem. Mater.*, 2015, **27**, 6535–6542.
34 Z. Xu, D. Hean, C. Climent, D. Casanova and M. O. Wolf, *Mater. Adv.*, 2021, **2**, 5777–5784.
35 D. J. Kim, K. H. Oh and J. K. Park, *Green Chem.*, 2014, **16**, 4098–4101.
36 R. Crespo-Otero, Q. Li and L. Blancafort, *Chem. – Asian J.*, 2019, **14**, 700–714.
37 H. Zhang, Z. Zhao, A. T. Turley, L. Wang, P. R. McGonigal, Y. Tu, Y. Li, Z. Wang, R. T. K. Kwok, J. W. Y. Lam and B. Z. Tang, *Adv. Mater.*, 2020, **32**, 2001457.
38 F. B. Dias, *Philos. Trans. R. Soc., A*, 2015, **373**, 20140447.
39 V. Jankus, E. W. Snedden, D. W. Bright, V. L. Whittle, J. A. G. Williams and A. Monkman, *Adv. Funct. Mater.*, 2013, **23**, 384–393.